

Preclinical Evaluation of a Fluorine-18 Labeled Probe for the Detection of the Expression of PSMA Level in Cancer

Yirui Guo, Dingyao Gao, Yinfei Chen, Yu Zhang, Liping Chen, Yong Mao, Chunjing Yu,* Ling Qiu, and Jianguo Lin*



Cite This: *ACS Omega* 2021, 6, 8279–8287



Read Online

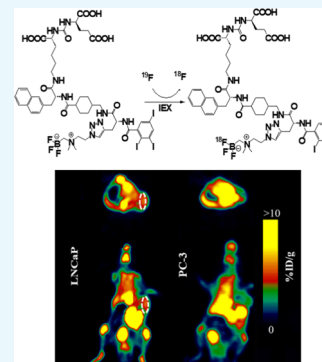
ACCESS |

Metrics & More

Article Recommendations

Supporting Information

ABSTRACT: Prostate-specific membrane antigen (PSMA) is a prospect biomarker for the treatment of prostate cancer. Meanwhile, positron emission tomography (PET) is being developed as a significant imaging modality in cancer diagnosis. A new PET probe Glu-ureido-Lys-naphthylalanine-tranexamic acid-Gly(AMBF₃)-triiodobenzoic acid (¹⁸F-GLNTGT) was radiosynthesized by a one-step ¹⁸F-labeled method. ¹⁸F-GLNTGT was obtained with a radioactivity yield (RCY) of 12.16 ± 6.4% and a good radiochemical purity (RCP > 96%). The cell uptakes of ¹⁸F-GLNTGT were determined to be 15.9 ± 0.43% ID and 9.47 ± 1.26% ID at 15 min in LNCaP cells and PC-3 cells, respectively. The cell internalization of ¹⁸F-GLNTGT was determined to be 12.89 ± 0.94% ID and 5.34 ± 0.15% ID at 15 min in LNCaP cells and PC-3 cells, respectively. It is suggested that the probe has good specificity targeting PSMA. From the results of ¹⁸F-GLNTGT binding affinity with PSMA, it has a higher affinity and a K_i value of 0.49 nM (95% confidence interval (CI): 0.35–0.67 nM). In PET imaging, ¹⁸F-GLNTGT showed the highest tumor uptake of 3.51 ± 0.15% ID/g at 45 min and the maximum tumor/muscle (T/M_{max}) ratio of 3.68 ± 0.29 at 60 min post-injection (p.i.) in LNCaP tumors. The control probe ¹⁸F-AIF-NOTA-RGD₂ presented the highest tumor uptake of 4.2 ± 0.54% ID/g at 7.5 min and the T/M_{max} ratio of 2.72 ± 0.63 at 45 min p.i. in LNCaP tumors. The results showed that the probe has a higher tumor/muscle ratio compared with the control probe ¹⁸F-AIF-NOTA-RGD₂. Although the probe ¹⁸F-GLNTGT has some limitations for CT signal detection both in cells and *in vivo*, it is still a promising PET probe for targeting PSMA membrane protein.



INTRODUCTION

Prostate cancer is a normal malignant tumor all over the world, which has become the fifth primary inducements of cancer deaths among adult male.¹ Currently, the gold standard for clinical diagnosis of early prostate cancer is a combination of prostate-specific antigen (PSA) blood test and prostate biopsy. Meanwhile, a large number of imaging techniques have been applied to the diagnosis of prostate cancer, such as bone scan, computed tomography (CT) scan, magnetic resonance imaging (MRI), lymph node biopsy, position emission tomography (PET) scan, and so on.^{2–4} Among all of the clinical image techniques of diagnosis malignant tumors, CT imaging is widely applied because of its higher spatial resolution and anatomical imaging ability. However, the low soft tissue resolution is the disadvantage of CT imaging.⁵ PET probes are applied to image a variety of tumor biomarkers, which will further promote tumor diagnosis efficiency. Meanwhile, noninvasive *in vivo* PET/CT imaging is utilized to precisely ensure the location of tumor.⁶ Currently, the application of molecular imaging technology for prostate cancer is usually a combination of PET with the CT imaging technology to achieve early diagnosis and staging of tumors.⁷ For example, ¹¹C and ¹⁸F-choline probes and ¹¹C-acetic acid probes achieved accurate PET/CT imaging of prostate cancer

cell membrane and fatty acid metabolism. Furthermore, the diagnosis efficacies of the above two types of probes in diagnosing prostate cancer at different stages were still low.^{8,9} Recently, researchers have shown an increased interest in exploring biomarkers in connection with the presence or development of prostate cancer. Prostate-specific membrane antigen (PSMA) is a transmembrane protein, which is highly expressed in prostate cancer. It is expressed strongly in low-differentiated, metastatic, and androgen-independent prostate cancers.¹⁰ Therefore, PSMA is a promising biomarker in prostate cancer.

What have been shown in the recent studies is that PET probes targeting PSMA have been explored. Due to the low blood clearance and high background value of the first-generation PSMA targeting probe (¹⁸F-DCFBC), the second and third generations (¹⁸F-DCFPyL and ¹⁸F-PSMA-617/1007, respectively) were developed.^{11,12} Studies have been devoted

Received: December 31, 2020

Accepted: March 8, 2021

Published: March 17, 2021



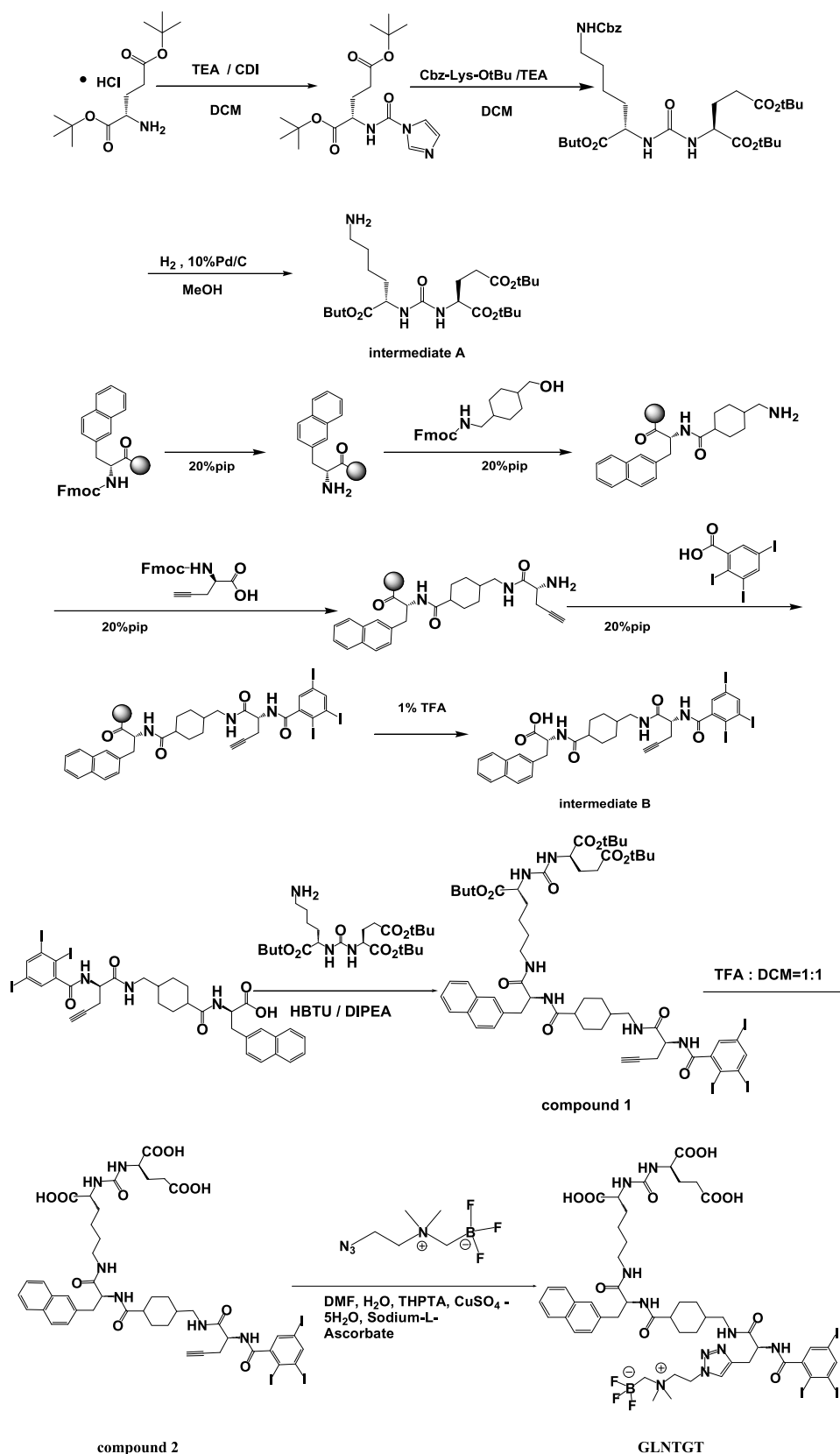


Figure 1. Synthesis of nonradioactive compound GLNTGT.

to developing PET imaging with targeting PSMA probes because of the higher detection effect of prostate cancer. Among these PSMA PET probes, ⁶⁸Ga-labeled targeting PSMA imaging probes have been used in prostate cancer

diagnosis.¹³ Although the ⁶⁸Ga-labeled targeting PSMA probes show good clinical imaging characteristics for prostate cancer, they have a shorter half-life and the rinsing quantities of the ⁶⁸Ga generator produce less isotopes. Fluoride-18 possesses an

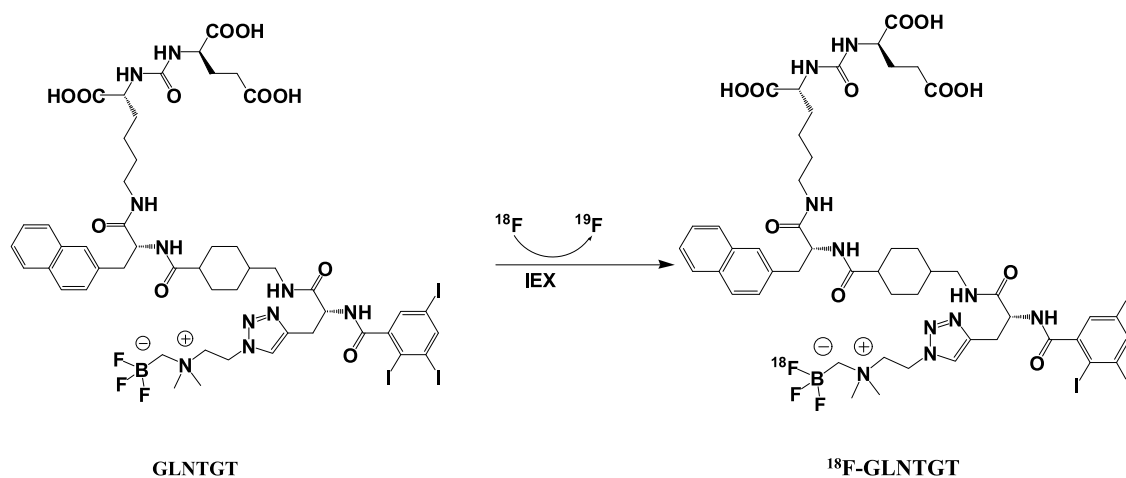


Figure 2. Radiochemical synthesis of probe ^{18}F -GLNTGT.

appropriate half-life, and larger doses are easily available; it is selected as a common radionuclide for prostate cancer.¹⁴

This study was focused on designing a probe targeting PSMA with higher competitive binding ability and achieving potential dual-modality imaging. The probe contains not only the glutamate-ureido-lysine scaffold bearing RBF_3^- radio-prosthetic groups for PET imaging¹⁵ but also the triiodobenzoic acid monomer group for CT signal detection.²¹ We measured the serum stability of probe and the $\log D_{7.4}$ value. The cell uptake, cytotoxicity, and competitive binding ability of the PSMA-targeted PET probe were evaluated in cells with different PSMA expression. Meanwhile, PET imaging of the probe in prostate cancer tumors with different PSMA expressions was performed. This further confirmed that the probe is a specific PET probe for imaging PSMA-overexpressed tumors.

RESULTS

Synthesis of Nonradioactive Compound GLNTGT.

The synthesis routes of nonradioactive compound GLNTGT are shown in Figure 1. We first synthesized intermediate A (yield: 460 mg, 95%) by the method reported in the literature.¹⁰ Intermediate B (yield: 410 mg, 88.2%) was synthesized by a solid-phase peptide synthesis method. The synthesis of compound 1 (yield: 140 mg, 49%) using intermediate A and intermediate B was performed at 25 °C in a N_2 atmosphere. Compound 2 (yield: 115 mg, 82.1%) could be obtained after compound 1 had been deprotected. Furthermore, the nonradioactive compound GLNTGT (yield: 20 mg, 40%) was obtained from the click reaction through compound 2. The electrospray ionization-mass spectrometry (ESI-MS), high-performance liquid chromatography (HPLC), ^1H , and ^{13}C nuclear magnetic resonance (NMR) characterizations of nonradioactive compound GLNTGT are shown in Figures S1–S11.

Radiosynthesis of ^{18}F -GLNTGT and *In Vitro* Stability Study. The probe ^{18}F -GLNTGT was obtained through a one-step ^{18}F -labeling reaction (Figure 2). The radiochemical yield of ^{18}F -GLNTGT was $12.16 \pm 6.4\%$. The specific activity of probe ^{18}F -GLNTGT was 31.71 ± 7.4 GBq/ μmol , and its radiochemical purity was over 96%. The probe ^{18}F -AIF-NOTA-RGD₂ was radiolabeled according to the literature.¹⁶ The stability of ^{18}F -GLNTGT was studied by radio-HPLC in phosphate buffered saline (PBS) and fetal bovine serum (FBS).

As can be seen in Figure 3, ^{18}F -GLNTGT was consistently stable in PBS and FBS during incubation for 4 h.

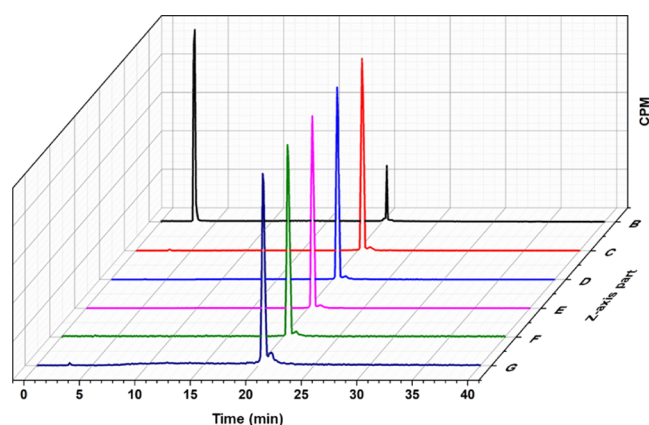


Figure 3. Meaning of the Z-axis part in the radiolabeling and stability diagrams: Line B represents the radioactive HPLC curve of probe ^{18}F -GLNTGT after radiolabeling; line C represents the radioactive HPLC curve of probe ^{18}F -GLNTGT after purification; lines D, E, and F represent the radioactive HPLC curves of probe ^{18}F -GLNTGT after 1, 2, and 4 h incubation in fetal bovine serum, respectively; line G represents the radioactive HPLC curve of the labeled substance after the probe ^{18}F -GLNTGT was incubated for 4 h in PBS.

Lipophilicity. The $\log D_{7.4}$ value of probe ^{18}F -GLNTGT was determined to be 0.39 ± 0.25 ($n = 3$), indicating that the probe was hydrophobic.

***In Vitro* Uptake Study and Cytotoxicity Determination.** The PSMA-mediated uptake of probe ^{18}F -GLNTGT was evaluated with LNCaP cells and PC-3 cells. As shown in Figure 4a, the cell uptake of probe ^{18}F -GLNTGT quickly increased to $15.90 \pm 0.43\%$ ID at 15 min and then slowly increased up to $17.61 \pm 1.71\%$ ID at 120 min in LNCaP cells. The cell uptake of probe ^{18}F -GLNTGT also gradually increased from $9.47 \pm 1.26\%$ ID at 15 min to $13.02 \pm 0.65\%$ ID at 120 min in PC-3 cells. The cytotoxicity of nonradioactive compound GLNTGT was determined in the prostate cancer cells with different PSMA expressions. As seen in Figure 4b, the cell viability of nonradioactive compound GLNTGT decreased slightly from 0.98 ± 0.02 at $6.25 \mu\text{M}$ to 0.92 ± 0.01 at $100 \mu\text{M}$ in LNCaP cells. The cell viability of nonradioactive compound GLNTGT

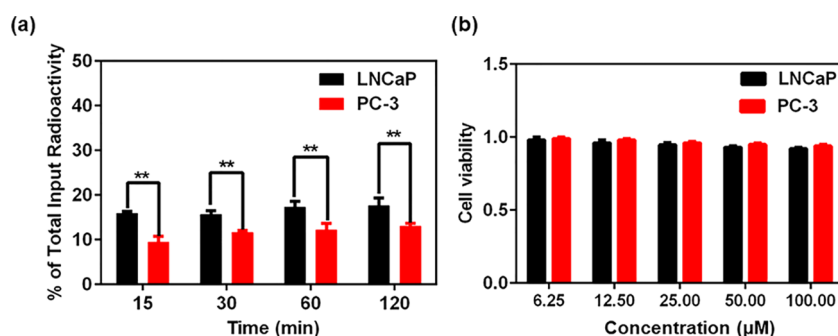


Figure 4. (a) Cell uptake assessment of probe ^{18}F -GLNTGT in LNCaP and PC-3 cells at 15, 30, 60, and 120 min ($*P < 0.05$, $**P < 0.01$, $***P < 0.001$). (b) Cytotoxicity assessment of nonradioactive compound GLNTGT in LNCaP and PC-3 cells at concentrations of 6.25, 12.5, 25, 50, and 100 μM .

also decreased slightly from 0.99 ± 0.01 at 6.25 μM to 0.94 ± 0.01 at 100 μM in PC-3 cells.

Cell Internalization. The cell internalization was performed to verify the specific targeting of the probe ^{18}F -GLNTGT in different PSMA expression cell lines. As shown in Figure 5, the internalization degree of probe ^{18}F -GLNTGT in

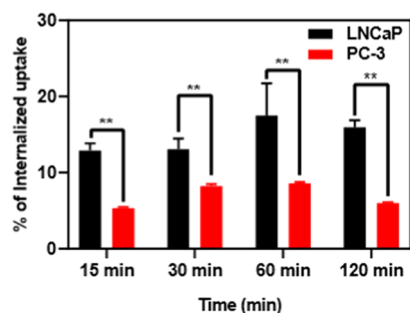


Figure 5. Cell internalization assessment of probe ^{18}F -GLNTGT in LNCaP and PC-3 cells at 15, 30, 60, and 120 min ($*P < 0.05$, $**P < 0.01$, $***P < 0.001$).

LNCaP cells gradually increased from $12.89 \pm 0.94\%$ ID at 15 min to $15.96 \pm 0.93\%$ ID at 120 min. The internalization degree of the probe ^{18}F -GLNTGT in PC-3 cells increased slightly from $5.34 \pm 0.15\%$ ID at 15 min to $6.01 \pm 0.10\%$ ID at 120 min. The results indicated that the probe has specific targeting to cells with different PSMA expressions.

Binding Assay. The inhibition constants (K_i) of probe ^{18}F -GLNTGT for PSMA were determined by the competitive binding method using LNCaP cells and the nonradioactive compound GLNTGT. As shown in Figure 6, as the concentration of the nonradioactive compound GLNTGT

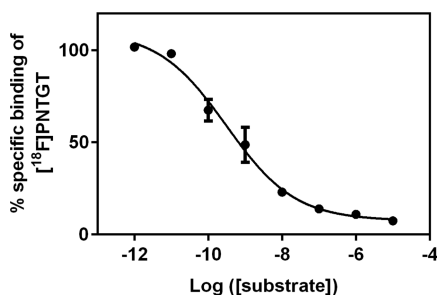


Figure 6. Competitive inhibition curve of probe ^{18}F -GLNTGT in LNCaP cells.

gradually increased, the competitive binding ability of the probe ^{18}F -GLNTGT to PSMA gradually decreased. Compared with the K_i value of ^{18}F -DCFPyL ($K_i = 2.0 \pm 0.8$),¹⁵ the K_i value of ^{18}F -GLNTGT (0.49 nM (95% confidence interval (CI): 0.35–0.67 nM)) was lower. This indicates that the probe ^{18}F -GLNTGT has better binding affinity to PSMA.

In Vitro CT Experiment. The CT values increased linearly with the concentration of the nonradioactive compound GLNTGT, and the CT images of the nonradioactive compound GLNTGT showed an obvious concentration-dependent brightening effect (Figure S13).

In Vivo PET Imaging. The high stability and specificity of ^{18}F -GLNTGT showed that this probe was fit for further *in vivo* experiments. As can be seen in the PET images in Figure 7a, uptake of the probe ^{18}F -GLNTGT was clearly observed in the LNCaP tumors from 15 to 60 min, and there was almost no uptake in the PC-3 tumors. The uptake curves of probe ^{18}F -GLNTGT in LNCaP and PC-3 tumors are shown in Figure 7b. The highest uptake of probe ^{18}F -GLNTGT in LNCaP tumor ($3.51 \pm 0.15\%$ ID/g at 45 min p.i.) showed a higher tumor uptake than the highest uptake of probe ^{18}F -GLNTGT in PC-3 tumors ($1.19 \pm 0.31\%$ ID/g at 15 min p.i.). The T/M ratios of probe ^{18}F -GLNTGT in LNCaP and PC-3 tumors are shown in Figure 7c. The T/M ratio of probe ^{18}F -GLNTGT in LNCaP tumors gradually increased ($T/M_{\text{max}} 3.68 \pm 0.29$ at 60 min p.i.) during the PET dynamic scanning time. The probe ^{18}F -GLNTGT reached the T/M_{max} ratio at 1.46 ± 0.39 at 30 min p.i., which then gradually decreased in PC-3 tumors.

As can be seen in the PET images in Figure S14a, the uptake of probe ^{18}F -AIF-NOTA-RGD₂ was clearly observed in both the LNCaP and PC3 tumors from 15 to 30 min p.i. The tumor uptake curves of probe ^{18}F -AIF-NOTA-RGD₂ in LNCaP and PC-3 tumors are shown in Figure S14b. The highest uptakes of probe ^{18}F -AIF-NOTA-RGD₂ in LNCaP and PC-3 tumors were $4.20 \pm 0.54\%$ ID/g and $5.70 \pm 0.79\%$ ID/g at 7.5 min p.i., respectively. The uptake of probe ^{18}F -AIF-NOTA-RGD₂ was significantly absorbed in LNCaP and PC-3 tumors during the PET dynamic scanning time. The T/M ratios of probe ^{18}F -AIF-NOTA-RGD₂ in LNCaP and PC-3 tumors are shown in Figure S14c. The T/M_{max} ratios of probe ^{18}F -AIF-NOTA-RGD₂ were 2.72 ± 0.63 at 45 min p.i. and 2.08 ± 0.79 at 15 min p.i. within LNCaP and PC-3 tumors, respectively.

DISCUSSION

The PET probe targeting PSMA with glutamate-ureido-lysine-naphthylalanine-tranexamic acid as the main structure has been extensively studied over the past years. Currently, the purpose

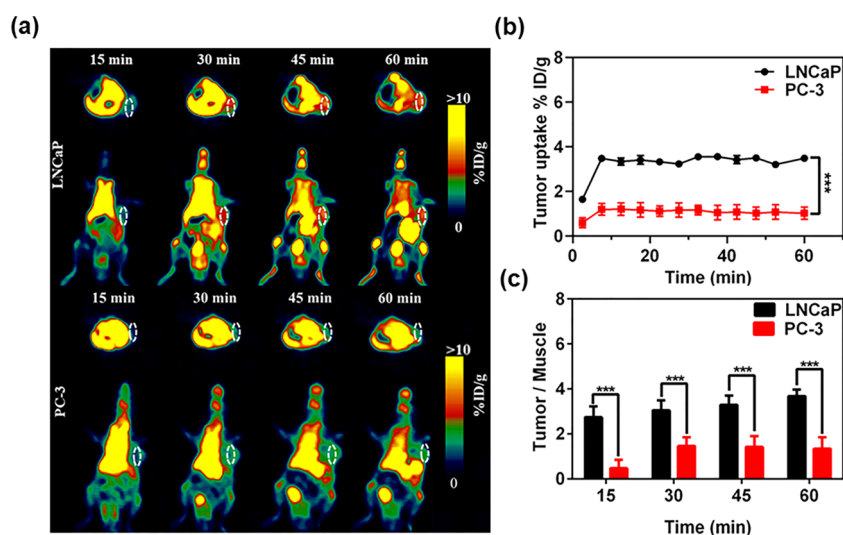


Figure 7. PET dynamic imaging in 60 min. The tumor nude mice were fixed and anesthetized (2% isoflurane mixed with oxygen), and then ^{18}F -GLNTGT (5.4–5.7 MBq) was injected through the tail vein. (a) PET dynamic imaging in 60 min of mice with the injection of ^{18}F -GLNTGT. (b) Average tumor uptake of the probe ^{18}F -GLNTGT in the whole tumor region of interest of LNCaP tumors and PC-3 tumors; (c) T/M ratios of ^{18}F -GLNTGT in LNCaP tumors and PC-3 tumors. Data were presented as mean \pm SD of $n = 3$ mice (* $P < 0.05$, ** $P < 0.01$, *** $P < 0.001$).

of modification of glutamate-ureido-lysine-naphthylalanine-tranexamic acid analogues is to increase tumor accumulation and expand the application range of probes.^{15,18–20,22} Meanwhile, since the triiodobenzoic acid monomer group is a common CT signal group,²¹ it is introduced into the glutamate-ureido-lysine-naphthylalanine-tranexamic acid structure to achieve PET/CT dual-modal imaging.

We measured some characterizations of probe ^{18}F -GLNTGT *in vitro* and *in vivo*. It is worth noting that the one-step ^{18}F -labeled method was easy to operate and shortened the production time. Therefore, nonradioactive compound GLNTGT was elected with this method to radiolabel. Meanwhile, the results indicated that ^{18}F -GLNTGT had good stability and could be further studied *in vitro* and *in vivo* experiments. The octanol–water partition coefficient was very important in the physicochemical properties of the probe, and it is reported to affect the pharmacokinetic parameters of the probe.²³ The octanol–water partition coefficient of probe ^{18}F -GLNTGT verified its hydrophobicity. Therefore, the above characteristics of probes contributed to the further study *in vitro* experiments.

The probe ^{18}F -GLNTGT has a very significant difference in cell uptake between LNCaP cells and PC-3 cells ($P < 0.01$), which indicated that the probe showed specificity toward prostate cancer cells with different PSMA expressions. The result of cell internalization can be further verified by the specific targeting of the probe. From the results of the cytotoxicity assay, nonradioactive compound GLNTGT at different concentrations had high cell viability in both LNCaP and PC-3 cells. The result indicated that the nonradioactive compound GLNTGT had better biocompatibility in cells with different PSMA expressions and was suitable for further *in vivo* experiments.²⁴ The binding affinity assay of probe ^{18}F -GLNTGT showed that the binding affinity of the probe to PSMA also reached to subnanomolar level after being modified with an iodine-containing group. This result verifies that probe ^{18}F -GLNTGT has achieved the design intention of improving the competitive binding ability with PSMA.¹⁵ Furthermore, considering that the structure of ^{18}F -GLNTGT contained a

triiodobenzoic acid monomer group,²¹ the nonradioactive compound GLNTGT might have potential CT signals. From the results of *in vitro* CT imaging, the nonradioactive compound GLNTGT has CT signal only at very high concentrations. Therefore, it is not possible to inject a large dose of nonradioactive compound GLNTGT through the tail vein to achieve CT signal detection *in vivo* because of the hydrophobicity of the probe.

Since ^{18}F -AIF-NOTA-RGD₂ targeted the integrin $\alpha v \beta_3$, it normally has high expression on the neovascularization of malignant tumors.¹⁶ Meanwhile, PSMA is also expressed in the neovascularization of malignant solid tumors but not in normal vasculature.^{25,26} Therefore, ^{18}F -AIF-NOTA-RGD₂ was chosen as a control probe to conduct a comparative study of PET imaging with probe ^{18}F -GLNTGT. To evaluate the diagnostic effect of the probes ^{18}F -GLNTGT and ^{18}F -AIF-NOTA-RGD₂ in the prostate cancer tumors with different PSMA expressions, PET imaging was performed in mice having prostate cancer tumors with different PSMA expressions. According to the results of micro-PET image, the probe ^{18}F -GLNTGT and the control probe ^{18}F -AIF-NOTA-RGD₂ were both uptaken in LNCaP tumors. However, the tumor uptakes of probe ^{18}F -GLNTGT and control probe ^{18}F -AIF-NOTA-RGD₂ in PC-3 tumors were completely different. It is suggested that the uptake of probe ^{18}F -GLNTGT could be distinguished accurately in prostate cancer tumors with different PSMA expressions compared to probe ^{18}F -AIF-NOTA-RGD₂ (Figures 7a and S14a). As shown in Figures 7b and S14b, the uptake of probe ^{18}F -GLNTGT was significantly different ($P < 0.001$) in prostate cancer tumors with different PSMA expressions. Although the control probe ^{18}F -AIF-NOTA-RGD₂ had higher tumor uptake than ^{18}F -GLNTGT, there was no extremely significant difference in prostate cancer tumors with different PSMA expressions ($P > 0.001$). Figures 7c and S14c show that the T/M ratios of the probe ^{18}F -GLNTGT were significantly increased in prostate cancer tumors with different PSMA expressions, while the T/M ratio of the control probe ^{18}F -AIF-NOTA-RGD₂ kept decreasing slowly. ^{18}F -GLNTGT was a hydrophobic probe, which undergoes defluorination of AMBF₃ labeling method, thus resulting in the probe ^{18}F -GLNTGT

with high uptake in nonspecific organs (mainly in metabolic organs such as liver, kidney, and intestine). However, these problems will not affect the uptake of probe ^{18}F -GLNTGT in tumors and the accurate distinction between tumors and normal tissues. The probe could be used for the noninvasive detection of PSMA level *in vivo*, which is considered a promising probe for the diagnose of prostate cancer.

CONCLUSIONS

Using a one-step ^{18}F -labeled method, a probe targeting PSMA with higher competitive binding capacity was designed and synthesized by click reaction between AMBF_3 and the corresponding alkyne precursors. Since the probe had good stability *in vitro*, it is appropriate for subsequent *in vitro* and *in vivo* experiments. The nonradioactive compound GLNTGT showed good biocompatibility in prostate cancer cells with different PSMA expressions. The cell internalization of ^{18}F -GLNTGT determined that the probe ^{18}F -GLNTGT has higher tumor cell uptake. Compared to probe ^{18}F -DCFPyL,¹⁴ the probe ^{18}F -GLNTGT has higher binding affinity to PSMA. The results of PET imaging indicated that the mice of the ^{18}F -GLNTGT group showed a higher T/M ratio than those of the control probe ^{18}F -AlF-NOTA-RGD₂. The probe holds promising candidates for PET imaging of prostate cancer.

EXPERIMENTAL SECTION

Materials. The reagents and solvents used in this study were purchased from the Bide Pharmatech Co., Ltd., SAAN Chemical Technology Co., Ltd., Sangon Biotech Shanghai Co., Ltd., Sinopharm Chemical Reagent Co., Ltd., and Sigma-Aldrich Co., Ltd. ^1H NMR spectra were recorded on a Bruker Ultrashield 400 MHz spectrometer. Mass spectrometric information for the synthetic intermediates of the nonradioactive compound GLNTGT was obtained by electrospray ionization mass spectrometry system (ESI-MS, Waters). The analytical high-performance liquid chromatography (1525, HPLC, Waters) and semipreparative HPLC (2545, Waters) of the nonradioactive compound GLNTGT were performed by the Breeze2 system. The analytical HPLC and semipreparative HPLC conditions are listed in Tables S1 and S2. Radioactivity was measured in a dose calibrator (CRC-15R, Capintec). The CT imaging of the nonradioactive compound GLNTGT was performed using a Micro-CT (MCT-1113, Suchow Hejun Technology Development Co., Ltd., China).

Synthesis of Nonradioactive Compound GLNTGT.

Synthesis of Compound 1. Intermediates A and B were obtained according to the previous report.⁸ *O*-Benzotriazole-*N,N,N',N'*-tetramethyl-uronium-hexafluorophosphate (HBTU) (72 mg, 0.19 mmol), *N,N*-dimethylformamide (DMF) (5 mL), intermediate A (100 mg, 0.20 mmol), and intermediate B (150 mg, 0.16 mmol) were added to a flask (50 mL). *N,N*-diisopropylethylamine (DIPEA) (80 μL , 0.47 mmol) was added to the reaction solution to adjust the pH to 8–9. After stirring at 25 $^\circ\text{C}$ for 3 h under nitrogen, the reaction product was dried under vacuum. The product was distilled by column chromatography (silica gel, $\text{CHCl}_3/\text{MeOH}$ = 100:3). Compound 1 (140 mg, 49%) was obtained and directly used for the next reaction. ESI-MS (m/z): calculated for $\text{C}_{37}\text{H}_{76}\text{I}_3\text{N}_6\text{O}_{11}$ ($[\text{M} + \text{H}]^+$) = 1401.27, observed as 1400.93.

Synthesis of Compound 2. Compound 1 was mixed with trifluoroacetic acid (TFA) (3 mL), CH_2Cl_2 (3 mL), and

triisopropylsilane (TIPS) (0.3 mL) in a round-bottom flask (25 mL). The mixture was reacted at room temperature for 1 h and then evaporated under vacuum to obtain compound 2 (115 mg, 82.1%). ESI-MS (m/z): calculated for $\text{C}_{45}\text{H}_{52}\text{I}_3\text{N}_6\text{O}_{11}$ ($[\text{M} + \text{H}]^+$) = 1233.08; observed as 1232.95.

Synthesis of Nonradioactive Compound GLNTGT. Compound 2 (50 mg, 0.04 mmol), ammoniomethyl-trifluoroborate (AMBF_3) (31 mg, 0.16 mmol), $\text{CuSO}_4 \cdot 5\text{H}_2\text{O}$ (5 mg, 0.02 mmol), tris(3-hydroxypropyltriazolylmethyl)amine (THPTA) (9 mg, 0.02 mmol), and sodium *L*-ascorbate (8 mg, 0.04 mmol) were dissolved in a mixture solvent ($\text{DMF}/\text{H}_2\text{O}$ = 4:1). The reaction mixture was stirred at room temperature for 30 min under nitrogen. After reaction, the nonradioactive compound GLNTGT (20 mg, 40%) was obtained by semipreparative HPLC purification using water–acetonitrile with 0.1% TFA as the eluent. ^1H NMR (400 MHz, dimethyl sulfoxide (DMSO)) δ 8.80 (dd, J = 23.4, 8.1 Hz, 1H), 8.24 (dd, J = 21.6, 16.4 Hz, 1H), 8.10–7.85 (m, 2H), 7.92–7.64 (m, 3H), 7.75–7.64 (m, 1H), 7.55–7.27 (m, 2H), 6.33 (t, J = 8.7 Hz, 1H), 4.84 (dd, J = 14.8, 7.6 Hz, 1H), 4.73–4.42 (m, 1H), 4.16–3.94 (m, 1H), 3.73 (dt, J = 13.5, 6.8 Hz, 1H), 3.59 (ddd, J = 35.0, 20.7, 14.2 Hz, 3H), 3.21–3.04 (m, 5H), 2.95 (dd, J = 22.9, 16.6 Hz, 6H), 2.71 (d, J = 16.8 Hz, 1H), 2.53 (d, J = 18.9 Hz, 6H), 2.46–2.19 (m, 2H), 2.07 (s, 1H), 1.69–1.54 (m, 2H), 1.49 (d, J = 6.2 Hz, 1H), 1.26 (d, J = 6.6 Hz, 13H), 1.18 (t, J = 7.3 Hz, 3H), 0.90–0.72 (m, 1H). ^{13}C NMR (101 MHz, DMSO) δ 127.83 (d, J = 16.2 Hz), 53.91 (s), 53.56 (s), 44.08 (d, J = 13.0 Hz), 42.19 (s), 40.61 (s), 40.40 (s), 40.13 (d, J = 13.2 Hz), 39.99 (s), 39.79 (s), 39.68 (d, J = 18.9 Hz), 39.46 (d, J = 21.0 Hz), 38.79 (d, J = 15.5 Hz), 30.22–29.45 (m), 29.20 (s), 12.83 (s). ESI-MS (m/z): calculated for $\text{C}_{50}\text{H}_{62}\text{BF}_3\text{I}_3\text{N}_{10}\text{O}_{11}$ ($[\text{M} - \text{H}]^-$) = 1427.18; observed as 1426.96.

Radiosynthesis of ^{18}F -GLNTGT. No carrier added ^{18}F -fluoride (7.4 GBq) was obtained by medical cyclotron (HM-7, Sumitomo Heavy Industries, Ltd., Japan) to bombard high-pressure ^{18}O -water targets with 18 MeV protons and rinsed with pyridazine buffer ($V_{\text{water}}/V_{\text{pyridazine}}$ = 3.3:1, 300 μL) directly into a centrifuge tube containing nonradioactive compound GLNTGT in DMF solution (25 mM, 30 μL). The mixture was incubated for 30 min at 80 $^\circ\text{C}$. The radioactive HPLC was used to detect the successful labeling of ^{18}F -GLNTGT. The labeled ^{18}F -GLNTGT reaction mixture was transferred to a 40 mL centrifuge tube with 20 mL of deionized water. The C18 light cartridge was rinsed twice (10 mL/time) with the mixture in the centrifuge tube. The residual radioactive dose of C18 light cartridge was measured after each wash. The C18 light cartridge was washed using 500 μL of ethanol in a 10 mL vial. The radiochemical purity of the probe was measured by radioactive HPLC.

Serum Stability Study. The probe ^{18}F -GLNTGT (20 μL at 0.074 MBq) was added into different centrifuge tubes containing fetal bovine serum (90 μL) and phosphate-buffered saline (PBS, pH = 7.4) (90 μL), respectively. The centrifuge tubes were then incubated for 1, 2, and 4 h at 37 $^\circ\text{C}$. Incubation samples (10 μL) were collected at each time point, and 10 μL of acetonitrile was added to each sample to precipitate the serum proteins. The incubation samples were centrifuged (12 000 rpm, 1 min) to obtain the supernatant for radio-HPLC analysis. The radio-HPLC analysis method of the supernatant is shown in Table S1.

Lipophilicity. The lipophilicity of probe in saturated octanol-deionized water (pH 7.4) was determined by the

shake flask method. In short, ^{18}F -GLNTGT was added to a centrifuge tube containing *n*-octanol (5 mL) and deionized water (5 mL). The mixture was shaken for 3 min and then centrifuged at 3000 rpm for 5 min. An aliquot of the mixture solution of the octanol (5 mL) and deionized water (5 mL) was counted by a γ -counter (2480, Perkin Elmer). $\log D_{7.4}$ was calculated by the formula: $\log D_{7.4} = \log_{10} [(\text{counts in } n\text{-octanol phase}/\text{counts in water phase})]$.

Cell Culture and Animal Models. Human prostate cancer LNCaP cell line and PC-3 cell line were purchased from the Cell Bank of the Chinese Academy of Sciences (Shanghai, China). The cells were cultured in RPMI-1640 medium added to 10% FBS, penicillin (100 U/mL), and streptomycin (100 $\mu\text{g}/\text{mL}$) as double antibody at 37 °C in a 5% CO_2 incubator (3111, Thermo Scientific). Cells achieving 80–90% confluence were washed with PBS and passaged with trypsin digestion. The collected cell number was counted by a cell counting plate. The male SCID mice (4–5 weeks old, 15–20 g) were purchased from Cavens Laboratory Animal Co., Ltd. (Changzhou, China) for the animal experiment. The SCID male mice were divided into two groups (three mice each group) and maintained under a specific pathogen-free (SPF) environmental condition for 1 week. LNCaP and PC-3 cell suspensions (5×10^6 cells in 200 μL per mouse) were implanted subcutaneously in the right armpit of mice from different groups, respectively. Tumor volumes were measured every other 2 days after injection until the appearance was observed in the tumors. The protocol of animal experiments was approved by the Animal Care and Ethics Committee of Jiangsu Institute of Nuclear Medicine.

Cell Uptake Studies. Cell uptake experiments were performed on LNCaP cells and PC-3 cells. The LNCaP cells and PC-3 cells were digested with 0.25% trypsin solution. According to the experimental protocols, the LNCaP cells ($1 \times 10^6/\text{tube}$) and PC-3 cells ($1 \times 10^6/\text{tube}$) were divided into centrifuge tubes ($1 \times 10^6/\text{tube}$). Then, ^{18}F -GLNTGT (100 μL at 0.037 MBq) was added to the centrifuge tubes containing the fresh medium. All samples were incubated for 15, 30, 60, and 120 min at 5% CO_2 and 37 °C. At each time point, the cells were washed in cold PBS (500 μL), centrifuged (12 000 rpm, 3 min), and the supernatant was discarded. The harvested cells were counted for their radioactivity by a γ -counter.

Cytotoxicity Determination. The prostate cancer cells with different PSMA expressions were digested with a 0.25% trypsin solution and 1640 medium containing 10% fetal bovine serum. The digestion cells were seeded in a 96-well plate. Each well was added with 100 μL of medium in the prostate cancer cells with different PSMA expressions ($8 \times 10^3/\text{well}$). The 96-well plate was incubated for 24 h at 37 °C in a 5% CO_2 incubator. According to the experimental protocols, the nonradioactive compound GLNTGT was set up in five concentration gradients (6.25, 12.5, 25, 50, 100 μM). Each concentration gradient was set up with six parallel groups. Nonradioactive compounds GLNTGT with different concentrations in the 96-well plate were placed for 24 h at 5% CO_2 in a 37 °C incubator. After incubated, the 3-(4,5-dimethylthiazol-2-yl)-2,5-diphenyl tetrazolium bromide (MTT) solution (5 mg/mL, 20 μL) was added to each well. Then, the 96-well plate was incubated for another 4 h at 37 °C in an incubator and the supernatant was discarded. Each well was added with DMSO (150 μL) and shaken for 15 min. Finally, the 96-well plate was measured by a microplate reader (BioTek, Inc., Vermont).

Cell Internalization. LNCaP cells ($1 \times 10^6/\text{tube}$) and PC-3 cells ($1 \times 10^6/\text{tube}$) that have been digested with 0.25% trypsin solution were added to the centrifuge tube, and then ^{18}F -GLNTGT (100 μL , 0.037 MBq) were added to centrifuge tubes containing fresh medium. The samples were placed at 37 °C in a 5% CO_2 incubator and incubated for 15, 30, 60, and 120 min. At each time point, cold PBS (4 °C, 500 μL) was added to the centrifuge tubes at different time points to stop the incubation, and then the used IP cell lysate was fully lysed, centrifuged at 12 000 rpm for 5–8 min, and the supernatant was obtained. The supernatant was counted externally, and the two types of cell pellets were internalized.²⁷

Competition Binding Assays. LNCaP cells were seeded on six-well plates and incubated for 48 h ($4 \times 10^5/\text{well}$). After incubating, the *N*-(2-hydroxyethyl)piperazine-*N'*-ethanesulfonic acid (HEPES) buffer (50 mM, pH 7.4, 0.9% NaCl) was replaced to ensure complete removal of the medium. After 1 h, different wells (in triplicate) contained various concentrations (0.01 nM to 100 μM) of the nonradioactive compound GLNTGT solution, to which an equal concentration of ^{18}F -GLNTGT (0.1 nM) was added. The assay mixture was incubated for 60 min at 37 °C in a 5% CO_2 incubator with slight shaking, and it was washed twice with HEPES buffer. A trypsin solution was put in each well to collect cells.²⁸ Radioactivity was measured by a γ -counter, and then the K_i value was calculated by GraphPad Prism 8.0 software.

In Vitro CT Imaging. The nonradioactive compound GLNTGT was divided into different concentration gradients (0–350 mM) with DMF. Micro-CT scanning was performed to determine the CT contrast effect in the nonradioactive compound GLNTGT of different concentrations. Imaging parameters were set as follows: thickness, 80 nm; voltage, 40 kV; current, 200 μA .¹⁷ The Hounsfield unit (*Hu*) values were determined by the Hiscan Viewer software.

PET Imaging Studies. The probe ^{18}F -GLNTGT with a specific activity of 5.4–5.7 MBq was injected through the tail vein into the prostate cancer xenograft tumor mice with different PSMA expressions, which had been fixed and anesthetized (2% isoflurane in oxygen). Dynamic (60 min) and static PET scans (10 min) were performed by a micro-PET scanner (Inveon, Siemens, Germany). After the scanning was completed, the PET image was reconstructed using a 2D ordered subset expectation maximization (2D-OSEM) algorithm and analyzed with Siemens IRW software. The percentage of per gram of tissue uptake (% ID/g) injected per gram of tumor and tissue was used for the semiquantitative assessment of the repeated dose for each region of interest (ROI). The imaging condition of the control probe ^{18}F -AlF-NOTA-RGD₂ was consistent with that of the probe ^{18}F -GLNTGT for PET imaging.

Statistical Analysis. All data of cell and animal experiments were expressed as mean \pm standard deviation (SD). The mean \pm SD values were compared by Student's *t* test; only *P* < 0.05 was considered statistically significant.

■ ASSOCIATED CONTENT

Supporting Information

The Supporting Information is available free of charge at <https://pubs.acs.org/doi/10.1021/acsomega.0c06353>.

Additional details on experimental methods, synthesis, radiolabeling methods, and *in vitro* and *in vivo* experiments (PDF)

AUTHOR INFORMATION

Corresponding Authors

Chunjing Yu – Wuxi School of Medicine, Jiangnan University, Wuxi 214122, P. R. China; Department of Nuclear Medicine, Affiliated Hospital of Jiangnan University, Wuxi 214062, P. R. China; Email: ycj_wxd1978@163.com

Jianguo Lin – NHC Key Laboratory of Nuclear Medicine, Jiangsu Key Laboratory of Molecular Nuclear Medicine, Jiangsu Institute of Nuclear Medicine, Wuxi 214063, P. R. China; orcid.org/0000-0003-1018-9794; Email: linjianguo@jsinm.org

Authors

Yirui Guo – Wuxi School of Medicine, Jiangnan University, Wuxi 214122, P. R. China; NHC Key Laboratory of Nuclear Medicine, Jiangsu Key Laboratory of Molecular Nuclear Medicine, Jiangsu Institute of Nuclear Medicine, Wuxi 214063, P. R. China

Dingyao Gao – NHC Key Laboratory of Nuclear Medicine, Jiangsu Key Laboratory of Molecular Nuclear Medicine, Jiangsu Institute of Nuclear Medicine, Wuxi 214063, P. R. China

Yinfei Chen – NHC Key Laboratory of Nuclear Medicine, Jiangsu Key Laboratory of Molecular Nuclear Medicine, Jiangsu Institute of Nuclear Medicine, Wuxi 214063, P. R. China

Yu Zhang – Department of Nuclear Medicine, Affiliated Hospital of Jiangnan University, Wuxi 214062, P. R. China

Liping Chen – Department of Nuclear Medicine, Affiliated Hospital of Jiangnan University, Wuxi 214062, P. R. China

Yong Mao – Department of Oncology, Affiliated Hospital of Jiangnan University, Wuxi 214062, P. R. China

Ling Qiu – NHC Key Laboratory of Nuclear Medicine, Jiangsu Key Laboratory of Molecular Nuclear Medicine, Jiangsu Institute of Nuclear Medicine, Wuxi 214063, P. R. China

Complete contact information is available at:
<https://pubs.acs.org/10.1021/acsomega.0c06353>

Notes

The authors declare no competing financial interest.

ACKNOWLEDGMENTS

This research was financially supported by the National Natural Science Foundation of China (81471691) and the Precision Medical Project of Wuxi Commission of Health and Family Planning (J201804).

REFERENCES

- (1) Siegel, R. L.; Miller, K. D.; Jemal, A. Cancer statistics, 2020. *CA: Cancer J. Clin.* **2020**, *70*, 7–30.
- (2) Kirby, R. Early detection the key to prostate cancer. *Practitioner* **2009**, *253*, 17–18.
- (3) Tikkinen, K. A. O.; Dahm, P.; Lytvyn, L.; Heen, A. F.; Vernooij, R. W. M.; Siemieniuk, R. A. C.; Wheeler, R.; Vaughan, B.; Fobuzi, A. C.; Blanker, M. H.; et al. Prostate cancer screening with prostate-specific antigen (PSA) test: a clinical practice guideline. *BMJ* **2018**, *362*, No. k3581.
- (4) Cuzick, J.; Thorat, M. A.; Andriole, G.; Brawley, O. W.; Brown, P. H.; Culig, Z.; Eeles, R. A.; Ford, L. G.; Hamdy, F. C.; Holmberg, L.; et al. Prevention and early detection of prostate cancer. *Lancet Oncol.* **2014**, *15*, e484–e492.
- (5) Kim, J.; Chhour, P.; Hsu, J.; Litt, H. I.; Ferrari, V. A.; Popovtzer, R.; Cormode, D. P. Use of Nanoparticle Contrast Agents for Cell Tracking with Computed Tomography. *Bioconjugate Chem.* **2017**, *28*, 1581–1597.
- (6) Han, Z.; Sergeeva, O.; Roelle, S.; Cheng, H.; Gao, S.; Li, Y.; Lee, Z.; Lu, Z. R. Preparation and Evaluation of ZD2 Peptide ⁶⁴Cu-DOTA Conjugate as a Positron Emission Tomography Probe for Detection and Characterization of Prostate Cancer. *ACS Omega* **2019**, *4*, 1185–1190.
- (7) Moawad, E. Isolated system towards a successful radiotherapy treatment. *Nucl. Med. Mol. Imaging* **2010**, *44*, 123–136.
- (8) Brogssitter, C.; Zophel, K.; Kotzker, J. ¹⁸F-Choline, ¹¹C-choline and ¹¹C-acetate PET/CT: comparative analysis for imaging prostate cancer patients. *Eur. J. Nucl. Med. Mol. Imaging* **2013**, *40*, S18–S27.
- (9) Vavere, A. L.; Kridel, S. J.; Wheeler, F. B.; Lewis, J. S. ¹¹C-acetate as a PET radiopharmaceutical for imaging fatty acid synthase expression in prostate cancer. *J. Nucl. Med.* **2008**, *49*, 327–334.
- (10) Bouvet, V.; Wuest, M.; Jans, H. S.; Janzen, N.; Genady, A. R.; Valliant, J. F.; Benard, F.; Wuest, F. Automated synthesis of [¹⁸F]DCFPyL via direct radiofluorination and validation in preclinical prostate cancer models. *EJNMMI Res.* **2016**, *6*, No. 40.
- (11) Cho, S. Y.; Gage, K. L.; Mease, R. C.; Senthamizchelvan, S.; Holt, D. P.; Jeffrey-Kwanisai, A.; Endres, C. J.; Dannals, R. F.; Sgouros, G.; Lodge, M.; et al. Biodistribution, Tumor Detection, and Radiation Dosimetry of ¹⁸F-DCFBC, a Low-Molecular-Weight Inhibitor of Prostate-Specific Membrane Antigen, in Patients with Metastatic Prostate Cancer. *J. Nucl. Med.* **2012**, *53*, 1883–1891.
- (12) Szabo, Z.; Mena, E.; Rowe, S. P.; Plyku, D.; Nidal, R.; Eisenberger, M. A.; Antonarakis, E. S.; Fan, H.; Dannals, R. F.; Chen, Y.; et al. Initial Evaluation of [¹⁸F]DCFPyL for Prostate-Specific Membrane Antigen (PSMA)-Targeted PET Imaging of Prostate Cancer. *Mol. Imaging Biol.* **2015**, *17*, S65–S74.
- (13) Haberkorn, U.; Kopka, K.; Hadaschik, B. Positron Emission Tomography-computed Tomography with Prostate-specific Membrane Antigen Ligands as a Promising Tool for Imaging of Prostate Cancer. *Eur. Urol.* **2016**, *69*, 397–399.
- (14) Dietlein, M.; Kobe, C.; Kuhnert, G.; Stockter, S.; Fischer, T.; Schomacker, K.; Schmidt, M.; Dietlein, F.; Zlatopolskiy, B. D.; Krapf, P.; et al. Comparison of [¹⁸F]DCFPyL and [⁶⁸Ga]Ga-PSMA-HBED-CC for PSMA-PET Imaging in Patients with Relapsed Prostate Cancer. *Mol. Imaging Biol.* **2015**, *17*, S75–S84.
- (15) Kuo, H. T.; Lepage, M. L.; Lin, K. S.; Pan, J.; Zhang, Z.; Liu, Z.; Pryyma, A.; Zhang, C.; Merckens, H.; Roxin, A.; et al. One-Step ¹⁸F-Labeling and Preclinical Evaluation of Prostate-Specific Membrane Antigen Trifluoroborate Probes for Cancer Imaging. *J. Nucl. Med.* **2019**, *60*, 1160–1166.
- (16) Liu, S.; Liu, H.; Jiang, H.; Xu, Y.; Zhang, H.; Cheng, Z. One-step radiosynthesis of ¹⁸F-ALF-NOTA-RGD₂ for tumor angiogenesis PET imaging. *Eur. J. Nucl. Med. Mol. Imaging* **2011**, *38*, 1732–1741.
- (17) Zou, Q.; Huang, J.; Zhang, X. One-Step Synthesis of Iodinated Polypyrrole Nanoparticles for CT Imaging Guided Photothermal Therapy of Tumors. *Small* **2018**, *14*, No. 1803101.
- (18) Eder, M.; Schafer, M.; Bauder-Wust, U.; Hull, W. E.; Wangler, C.; Mier, W.; Haberkorn, U.; Eisenhut, M. ⁶⁸Ga-complex lipophilicity and the targeting property of a urea-based PSMA inhibitor for PET imaging. *Bioconjugate Chem.* **2012**, *23*, 688–697.
- (19) Gregor, P. D.; Wolchok, J. D.; Turaga, V.; Latouche, J. B.; Sadelain, M.; Bacich, D.; Heston, W. D.; Houghton, A. N.; Scher, H. I. Induction of autoantibodies to syngeneic prostate-specific membrane antigen by xenogeneic vaccination. *Int. J. Cancer* **2005**, *116*, 415–421.
- (20) Yang, D.; Holt, G.; Velders, M.; Kwon, E.; Kast, W. Murine six-transmembrane epithelial antigen of the prostate, prostate stem cell antigen, and prostate-specific membrane antigen: prostate-specific cell-surface antigens highly expressed in prostate cancer of transgenic

adenocarcinoma mouse prostate mice. *Cancer Res.* **2001**, *61*, 5857–5860.

(21) Wang, A.; Yin, L.; He, L.; Xia, H.; Chen, F.; Zhao, M.; Ding, J.; Shi, H. An acidic pH/reduction dual-stimuli responsive nanoprobe for enhanced CT imaging of tumours in vivo. *Nanoscale* **2018**, *10*, 20126–20130.

(22) Zang, J.; Fan, X.; Wang, H.; Liu, Q.; Wang, J.; Li, H.; Li, F.; Jacobson, O.; Niu, G.; Zhu, Z.; et al. First-in-human study of ¹⁷⁷Lu-EB-PSMA-617 in patients with metastatic castration-resistant prostate cancer. *Eur. J. Nucl. Med. Mol. Imaging* **2019**, *46*, 148–158.

(23) Waterhouse, R. Determination of lipophilicity and its use as a predictor of blood-brain barrier penetration of molecular imaging agents. *Mol. Imaging Biol.* **2003**, *5*, 376–389.

(24) Chong, Y.; Chang, J.; Zhao, W.; He, Y.; Li, Y.; Zhang, H.; Qi, C. Synthesis and evaluation of novel ¹⁸F-labeled quinazoline derivatives with low lipophilicity for tumor PET imaging. *J. Labelled Compd. Radiopharm.* **2018**, *61*, 42–53.

(25) Conway, R.; Petrovic, N.; Li, Z.; Heston, W.; Wu, D.; Shapiro, L. Prostate-specific membrane antigen regulates angiogenesis by modulating integrin signal transduction. *Mol. Cell. Biol.* **2006**, *26*, 5310–5324.

(26) Wang, Y.; Li, Y.; Liu, X.; Lu, X.; Cao, X.; Jiao, B. Marine Antibody-Drug Conjugates: Design Strategies and Research Progress. *Mar. Drugs* **2017**, *15*, No. 18.

(27) Nedrow-Byers, J.; Jabbes, M.; Jewett, C.; Ganguly, T.; He, H.; Liu, T.; Benny, P.; Bryan, J.; Berkman, C. A phosphoramidate-based prostate-specific membrane antigen-targeted SPECT agent. *Prostate* **2012**, *72*, 904–912.

(28) Roxin, A.; Zhang, C.; Huh, S.; Lepage, M.; Zhang, Z.; Lin, K.; Bénard, F.; Perrin, D. A Metal-Free DOTA-Conjugated ¹⁸F-Labeled Radiotracer: [¹⁸F]DOTA-AMBF-LLP2A for Imaging VLA-4 Over-Expression in Murine Melanoma with Improved Tumor Uptake and Greatly Enhanced Renal Clearance. *Bioconjugate Chem.* **2019**, *30*, 1210–1219.